JOM, Vol. 68, No. 11, 2016
DOI: 10.1007/s11837-016-2042-7

Three Dimensional Characterization of Tin Crystallography and Cu_6Sn_5 Intermetallics in Solder Joints by Multiscale Tomography

A. KIRUBANANDHAM,[1] I. LUJAN-REGALADO,[1] R. VALLABHANENI,[1] and N. CHAWLA[1,2]

1.—Materials Science and Engineering, Arizona State University, Tempe, AZ 85287-5604, USA.
2.—e-mail: nchawla@asu.edu

Decreasing pitch size in electronic packaging has resulted in a drastic decrease in solder volumes. The Sn grain crystallography and fraction of intermetallic compounds (IMCs) in small-scale solder joints evolve much differently at the smaller length scales. A cross-sectional study limits the morphological analysis of microstructural features to two dimensions. This study utilizes serial sectioning technique in conjunction with electron backscatter diffraction to investigate the crystallographic orientation of *both* Sn grains and Cu_6Sn_5 IMCs in Cu/Pure Sn/Cu solder joints in three dimensional (3D). Quantification of grain aspect ratio is affected by local cooling rate differences within the solder volume. Backscatter electron imaging and focused ion beam serial sectioning enabled the visualization of morphology of both nanosized Cu_6Sn_5 IMCs and the hollow hexagonal morphology type Cu_6Sn_5 IMCs in 3D. Quantification and visualization of microstructural features in 3D thus enable us to better understand the microstructure and deformation mechanics within these small scale solder joints.

INTRODUCTION

Solder alloys have been used extensively in the electronics industry for several decades. The transition to Pb-free interconnects has increased the demand for Sn-rich solder alloys.[1] The development of three-dimensional (3D) packaging technologies and decreasing pitch size has significantly reduced the volume of solder spheres and interconnects in the package. While the Sn crystallography and distribution of intermetallic compounds (IMCs) of common alloys have been widely investigated,[2–4] the evolution of solder microstructure is not well understood, especially with decreasing length scale. This is largely due to the two-dimensional (2D) nature of microstructural analysis. In addition, at small length scales, the microstructure is highly heterogeneous and a statistical representative volume cannot be obtained to represent the properties of the solder joint.

In solder systems, Sn is the primary constituent and its body-centered tetragonal (BCT) structure is strongly anisotropic, making crystallographic orientation analysis extremely important. Indeed, Sn grain size, shape, orientation and texture have an important role in influencing solder reliability.[5]

Lehman et al.[6] studied the effect of miniaturization and showed that decreasing the solder volume increases the undercooling behavior. Randomly oriented "interlaced" areas were seen to appear more frequently. Dimensional constraints in such small-volume solder joints influence the mechanical properties, and several experimental[7,8] and numerical[9] studies have been conducted to investigate this effect. As the solder volume decreases, the bulk behavior is gradually lost, leading to a more orientation-dependent structure. This is because one would expect that, with the highly anisotropic behavior of Sn, as the volumes get smaller there will be a smaller number of grains. Thus, a particular grain orientation may be more influential in controlling the deformation behavior of that volume.[5]

A significant amount of work has been done on characterizing the crystallography of tin and the intermetallics in 2D, especially under conditions of electromigration and thermal fatigue. Recent work

(Published online July 28, 2016)

carried out by Mertens et al.[10,11] shows the volumetric evolution of Cu_6Sn_5 IMCs within the solder microstructure using x-ray tomography and electron backscatter diffraction (EBSD), and discusses the strong influence of orientation in estimating the effective diffusivity of Cu with respect to Sn a and c axes. Based on the x-ray tomography data, a large chunk of Cu_6Sn_5 IMC was seen to have formed within the solder volume during electromigration. This is a serious reliability issue and it would not have been identified unless a 3D characterization technique had been used. In such cases, to understand the performance and true behavior of a solder joint, 3D reconstruction, visualization, and quantification of the different microstructural features become necessary.

Among the several 3D characterization capabilities currently available, serial sectioning is a well-established technique to characterize and visualize the microstructure. Serial sectioning work carried out by Sidhu and Chawla[12] on Ag_3Sn intermetallic particle distribution showed the large deviation in IMC needle aspect ratios between 2D and 3D measurements. As the size of these IMCs were of the order of several microns, fine mechanical polishing and optical microscopy techniques were sufficient for reconstruction and 3D analysis. In order to resolve finer particles measuring less than a micron in diameter, a focused ion beam serial sectioning process can be utilized. Recent advancements in dual beam focused ion beam scanning electron microscopy (FIB-SEM) have greatly increased the rate of data collection and allow large datasets to be analyzed and visualized in 3D. A study on the influence of oxidation of trace amount of rare earth intermetallics ($RESn_3$ particles) in favoring whisker growth using a FIB serial sectioning approach revealed how large IMCs tend to grow whiskers and smaller IMC particles favor growth of hillock-type whiskers.[13]

Considering the complex structures of Sn grains and the Cu_6Sn_5 intermetallic distributed in the material, a methodology to perform 3D characterization study on *both* Sn crystallography and the size and distribution of the intermetallic particles has yet to be developed. The challenge here is that the Sn grains and Cu_6Sn_5 particles are present at different length scales. The present work utilizes crystallographic characterization by EBSD in conjunction with serial sectioning technique using mechanical and FIB polishing to obtain 3D experimental volumes of the different microstructural features. With these techniques, we were able to elucidate the microstructure of both the Sn grains and the Cu_6Sn_5 intermetallic needles and nanoparticles as a function of solidification on a copper substrate.

MATERIALS AND EXPERIMENTAL PROCEDURE

Cu/pure-Sn/Cu sandwich joints were prepared in this study. Sn solder spheres (99.99% purity; Indium, Ithaca, NY, USA) with a diameter of 250 μm were reflowed between two polished high-purity oxygen-free high-conductivity (OFHC) copper wires. A silicon v-groove assembly was used for solder reflow on a programmable hot plate. The sample stage is a multi-groove silicon wafer consisting of 3 grooves of different sizes capable of holding solder joints of sizes anywhere between 500 μm and 100 μm. The wafer stage was fabricated using photolithography and anisotropic KOH etching techniques, similar to the wafer stage described elsewhere.[14] These grooves enable us to maximize the alignment of the sample during reflow and also allow multiple samples to be reflowed simultaneously under identical conditions, thereby allowing us to maintain the same applied cooling rate for all specimens for a given reflow. The polished copper wire and solder sphere preforms were coated with a rosin-mildly-activated (RMA) flux (Indium) and reflowed to a peak temperature of 250°C (approximately 20°C above the melting point of Sn) with a soak time of 40 s. Samples were cooled at approximately 1.2°C s^{-1} after reflow by controlled cooling in a furnace (Fig. 1a). The fabricated butt joint solder samples were then cleaned using acetone followed by isopropanol and then mounted in graphite-based conductive epoxy mounts.

Samples were metallographically polished for EBSD analysis, using 0.3 μm alumina solution and 0.05 μm colloidal silica solution in the final polishing step. To monitor the section depth after each polishing cycle of serial sectioning, fiducial marks were made by a Vickers indenter on the copper wires on either side of the solder joint. The depth of material removal was calculated by measuring the change in indentation diameter, as described elsewhere.[12] Determining the distance between slices in serial sectioning depends on the size of the smallest feature being visualized. The solder microstructure revealed some of the smallest grains sizes to be between 6 μm and 8 μm. Hence a semi-automatic polisher was standardized to polish 2 μm per polishing cycle which gives about 3–4 sections per grain.

A scanning electron microscope (JEOL JSM-6100) equipped with an EBSD (TSL™-EDAX, Mahwah, NJ, USA) system was used to obtain EBSD patterns on the solder joint cross-sections. Orientation image mapping (OIM) was conducted with a step-size of 0.6 μm on the entire solder joint cross-section for every polishing step. OIM maps were analyzed using TSL OIM Data Collection and Analysis software. To reduce isolated noise in the OIM maps, a three-step cleaning process using 'neighbor CI correlation', 'grain dilation,' and 'single average orientation per grain' methods was followed. Repeating this process for every polished section, a stack of 2D OIM images are obtained which can be segmented and reconstructed to obtain the complete 3D experimental volume. Additionally, by performing backscattered imaging (BSE) at every polishing step, the IMC particle distribution can be obtained due to phase

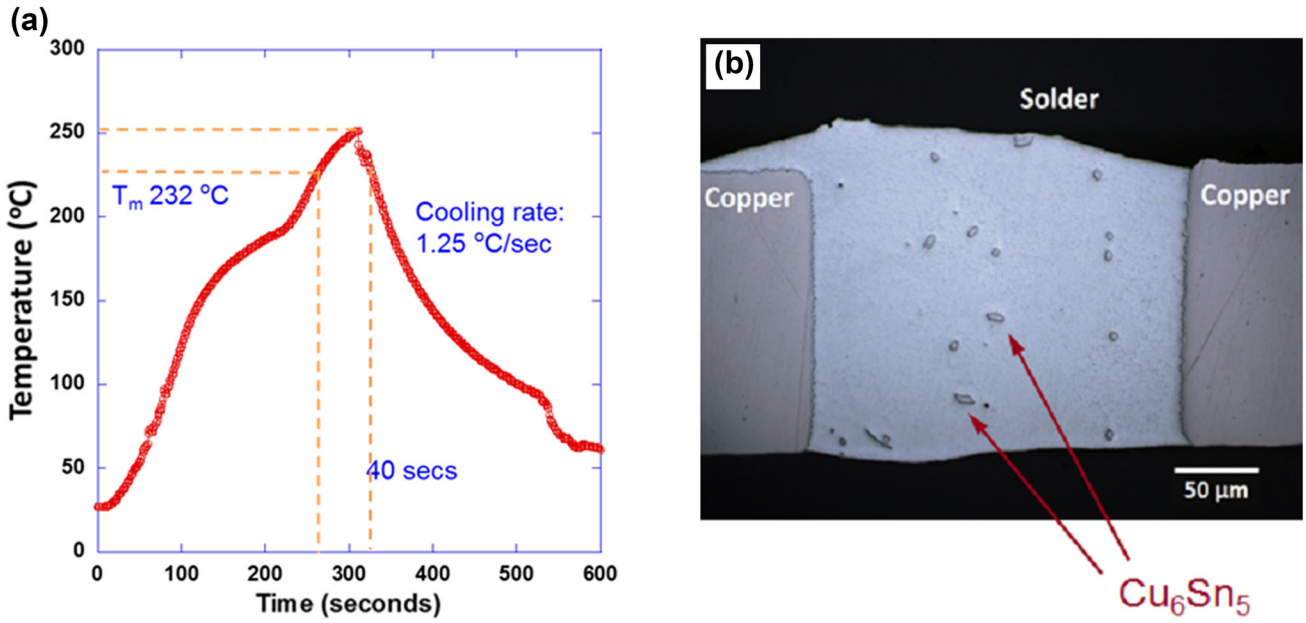

Fig. 1. (a) Reflow profile used to fabricate pure Sn solder joints. (b) Optical micrograph showing typical microstructural features in a 250-μm pure Sn solder joint.

contrast and this stack of 2D images can also be reconstructed into a 3D experimental volume. The segmentation of Sn grains and the IMC particles was done using a combination of grayscale processing using ImageJ (Bethesda, MD, USA) and 3D region growth and reconstruction using the Magic wand tool in Avizo® Fire software (VSG, Burlington, MA, USA) which was also used for visualization and 3D quantification analysis.

To visualize and quantify the true morphology of the nanosized Cu_6Sn_5 IMCs, FIB serial sectioning study was done at two volumes approximately 20 μm × 20 μm × 10 μm. During reflow, as Cu diffuses in Sn from the interfaces, the local compositional differences may influence the size and morphology of the Cu_6Sn_5 nanoparticles. To examine if such differences exist, one region close to the interface spanning several low-angle boundaries and the other region closer to the center of the solder joint was chosen for FIB serial sectioning. A dual beam focused ion beam scanning electron microscope (Nova 200 NanoLab FEG FIB-SEM; FEI, OR, USA) was used. An accelerating voltage of a 30-KeV Ga^+ ion beam with a 1-nA current was used to mill sections through the thickness and a final polishing with a 0.3-nA current was carried out to sequentially obtain a stack of 2D images. A thin layer of platinum (approximately 1 μm) was deposited on the surface to minimize FIB damage. A rectangular trench was milled out in front of the volume of interest, with a range of currents from 7 nA to 0.3 nA, to produce a clean cross-section through the thickness. Based on the size of the Cu_6Sn_5 nanoparticles (approximately 500–700 nm), sections were milled approximately 300 nm apart. A total of 30 sections were obtained and, after each milling step, ion channeling images were taken with the ion beam at a 0.1-nA current. Ion channeling images produce good contrast with the Cu_6Sn_5 IMCs and between certain grain orientations. These images were then used for segmentation, 3D reconstruction, and quantification.

RESULTS AND DISCUSSION

3D Sn Grain Orientation

The typical microstructural features in the solder volume can be seen in Fig. 1b. The majority phase in the joint is beta-Sn rich with a dispersion of fine Cu_6Sn_5 IMC nanoparticles and Cu_6Sn_5 needles with hexagonal cross-section. Secondary electron (SE) and BSE images with the corresponding OIM map of a single cross-section of a 250-μm pure Sn solder joint are shown in Fig. 2. The EBSD scan dimensions are 320 μm × 290 μm with a lateral step size of 0.6 μm and a total of 65 OIM slices. The EBSD maps indicate the grain orientation normal (ND) to the solder sample surface. A dispersion of Cu_6Sn_5 nanoscale IMCs, about 300 nm in diameter, segregated both at the grain boundaries and within the Sn grains. Apart from the nanoparticles, several Cu_6Sn_5 IMC needles were also observed within the solder volume, indicated by red arrows in Fig. 2b. These IMC needles were seen to have hexagonal cross-section and often had hollow cores. Work by Frear et al.[15] explains that these IMC needles form when molten Sn comes in contact with Cu, forming hexagonal rods along a screw dislocation using a ledge mechanism. Due to the turbulence in molten Sn during reflow, these rods break from the Cu

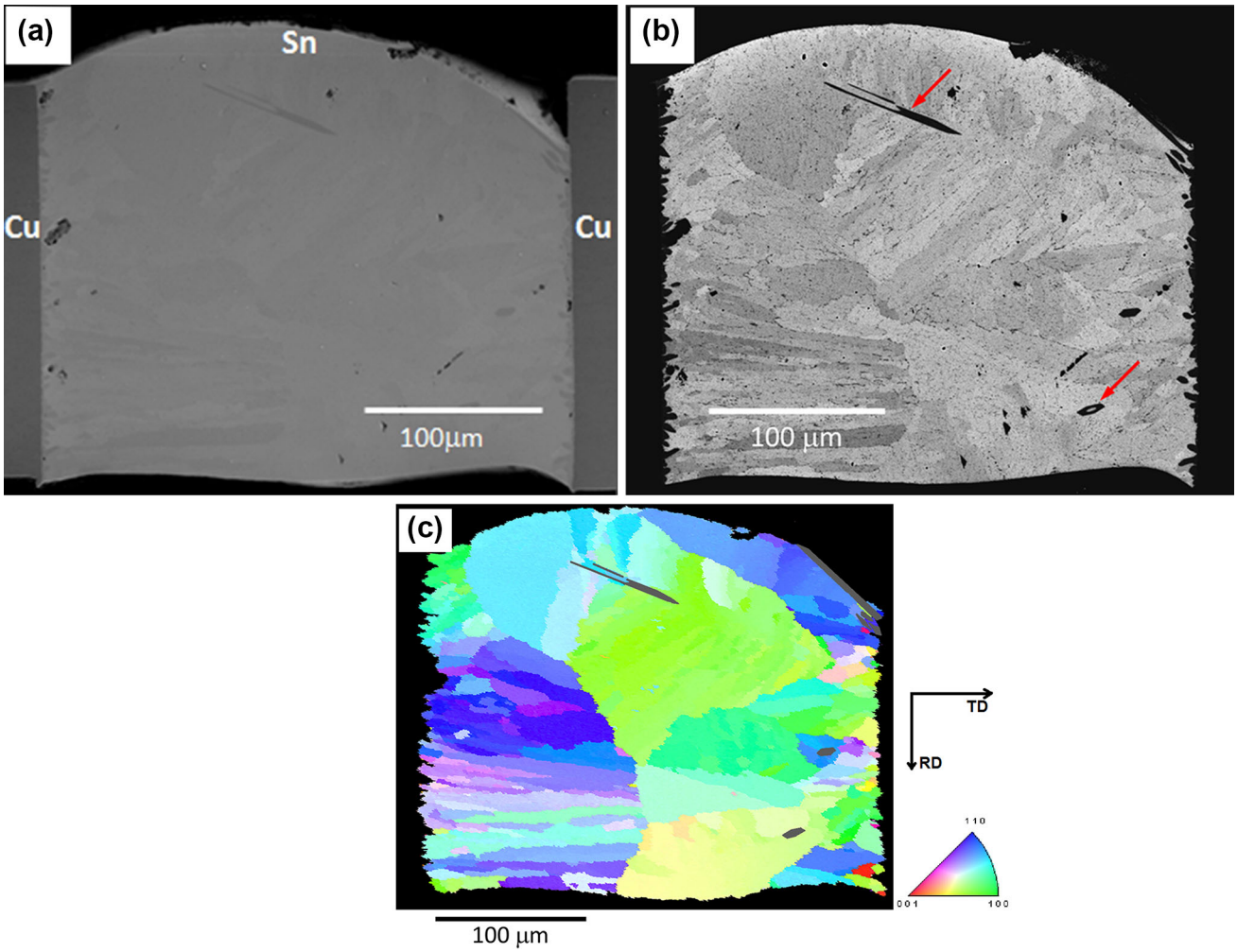

Fig. 2. (a) Secondary electron image. (b) Backscatter electron image. (c) OIM map of 250-μm pure Sn solder joint.

interface and drift into the solder volume, where a local deficiency of Cu tends to dissolve the rods from its high-energy sites, i.e., the screw dislocation core. Molten Sn flows into this hollow tube and eventually solidifies.

OIM analysis showed the presence of thinner elongated grains with the grain growth direction normal to the Cu interface on either side. This indicates a high local cooling rate influenced by the high thermal conductivity of copper. Grains closer to the center, however, are larger and more equiaxed indicating a limited heat flow and, thus, favoring more grain growth. The thin elongated grains were about 5–7 μm in width with the average length normal to the Cu interface exceeding 50 μm. The larger equiaxed grains in the center had an average grain size of 90 $\pm$ 20 μm.

Upon nucleation, the Sn grains grow rapidly and there can be growth competition between neighboring grains. Sn grains nucleate from the Cu/Sn interfaces and also from Cu_6Sn_5 IMC needles that form during reflow within the molten solder. However, the surface area of the Cu/Sn interface is much larger compared to the IMC needles and thus provides more nucleation sites.

The extent of local cooling rate differences within the solder volume was analyzed by measuring the aspect ratio of the Sn grains which were segmented, as shown in Fig. 3c. A 3D aspect ratio measurement as a function of position of grains from either Cu interface was plotted. The centroids of the grains were identified and the x-coordinates were used for assigning the grain position with respect to the left interface. A bimodal type trend was clearly seen with high aspect ratio grains ($>$4–5) present at either interface, with a few large equiaxed grains in the center, as shown in Fig. 4a.

The Sn grains showed extensive low-angle boundary formation with 38% of the grain boundaries having a misorientation angle less than 15°. The majority of these low-angle grain boundaries were present close to the interface which can be explained by the high local cooling rate. Also, it can be seen that there is a significant amount of

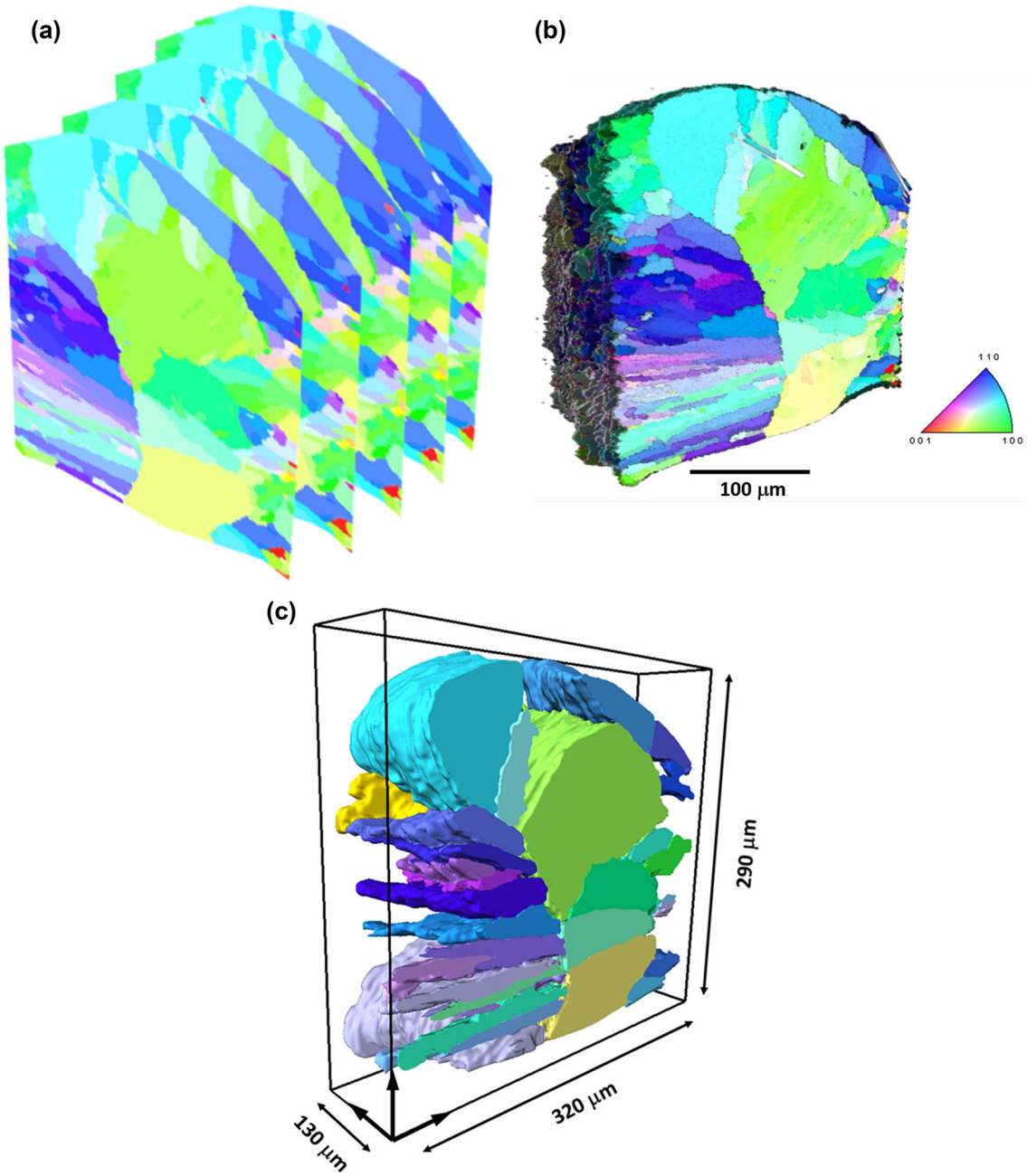

Fig. 3. (a) 2D OIM stack of the 250-μm solder joint and (b) 3D reconstructed volume of Sn grain orientation. (c) Segmented volume from the 3D dataset showing grains colored with respect to the OIM map and rendered in 3D though the thickness.

grain boundaries with rotation angles between 55° and 70°. This is common in Sn solder systems as twinning occurs during Sn solidification with twins forming on {1 0 1} and {3 0 1} crystal planes with twinning angles of 57.2° and 62.8°, respectively[16–18] (Fig. 5) (Table I).

Investigation of Cu_6Sn_5 IMCs

The mean IMC thickness at the Cu interfaces was approximately 3.7 ± 2 μm. The high standard deviation can be attributed to the scallop-type morphology of these intermetallics. The Cu_6Sn_5 nanoparticles were segmented in all 65 serial sections and were quantified in 3D. To enhance the contrast of these nanoparticles, a two-step filtering process using a band-pass filter followed by an anisotropic diffusion filter was used prior to grayscale thresholding. The volume fraction of these IMCs in the reconstructed volume was measured as 1.67%, and Fig. 6a shows the reconstruction in 3D.

The Cu_6Sn_5 IMC needles were also segmented, reconstructed and quantified in the same volume from BSE images as described in Ref. 19. Analysis

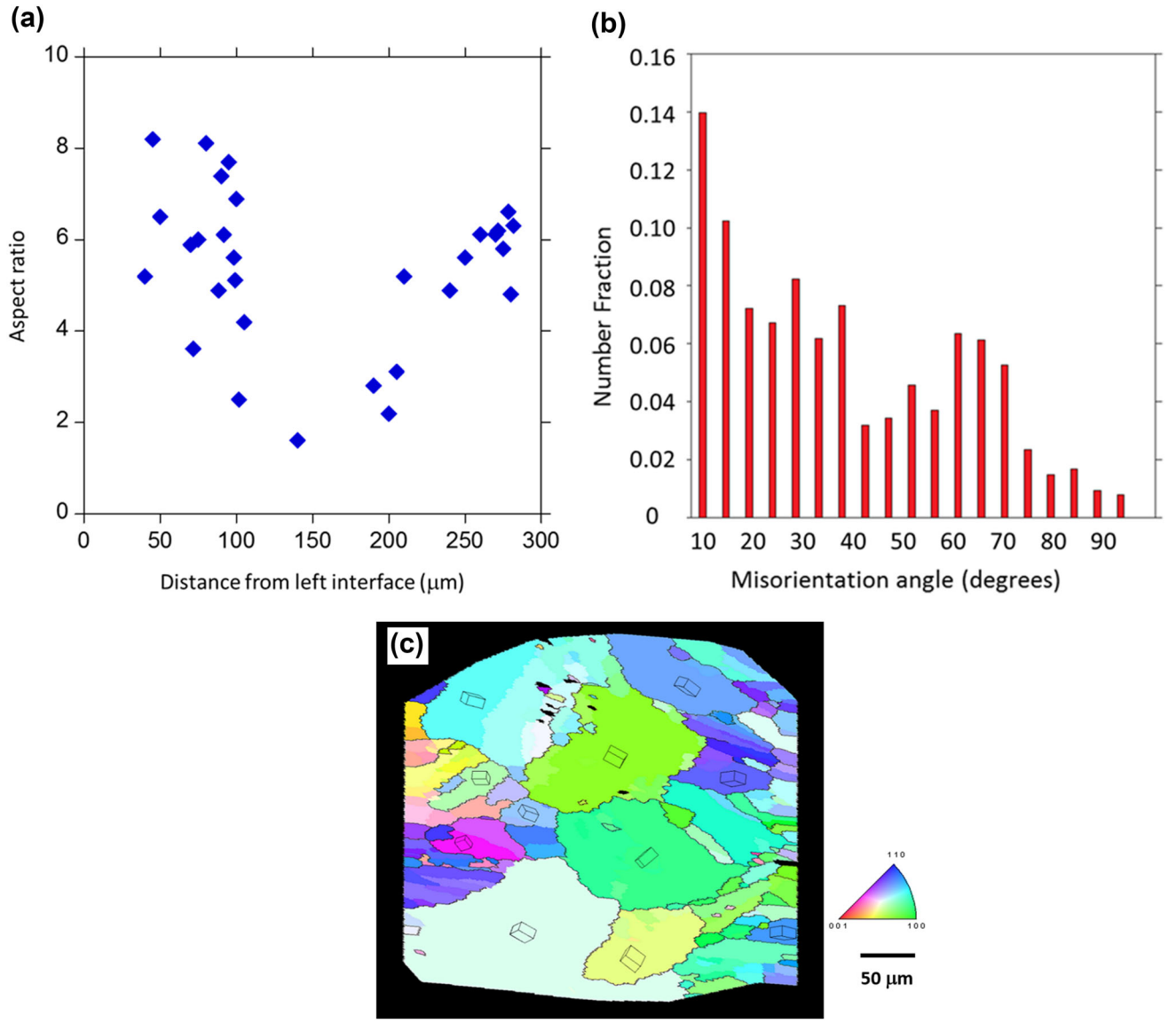

Fig. 4. (a) Aspect ratio plot showing the extent of formation of elongated grains. (b) Misorientation plot giving the distribution of grain boundary rotation angles within the solder volume. (c) OIM map of a single cross-section with high angle boundaries (>15°) highlighted in black.

Table I. 2D quantification results of the Cu_6Sn_5 nanoparticles

Area fraction	Mean area	Mean maximum feret diameter	Aspect ratio
2.18%	0.235 μm^2	0.69 μm	1.64

showed that the large IMCs had a high mean aspect ratio exceeding 3.4 and the results are given in Table II.

FIB cross-sectioning of the nano-sized Cu_6Sn_5 IMCs on two separate volumes in a 250-μm solder joint is shown in Fig. 7.

FIB cross-sectional analysis shows the nearly spherical morphology of the Cu_6Sn_5 nano-IMCs. Region 1 was extracted close to the Cu interface and it can be seen that the IMCs prefer to segregate at the grain boundaries, and hence have a directional arrangement perpendicular to the interface. Region

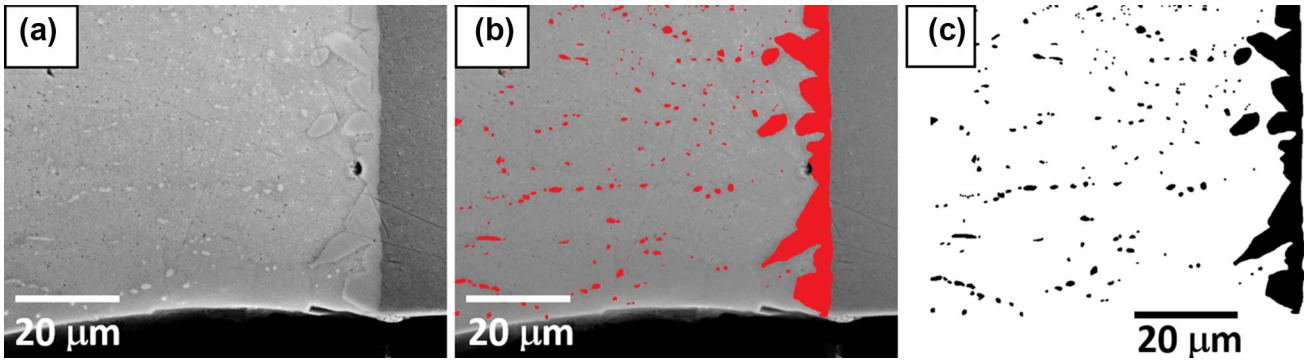

Fig. 5. Segmentation of Cu_6Sn_5 nanoparticles. (a) SE image of a magnified part of the solder cross-section. (b) Cu_6Sn_5 phases are selectively thresholded by their grayscale value. (c) Segmented Cu_6Sn_5 IMCs as black features in a white matrix.

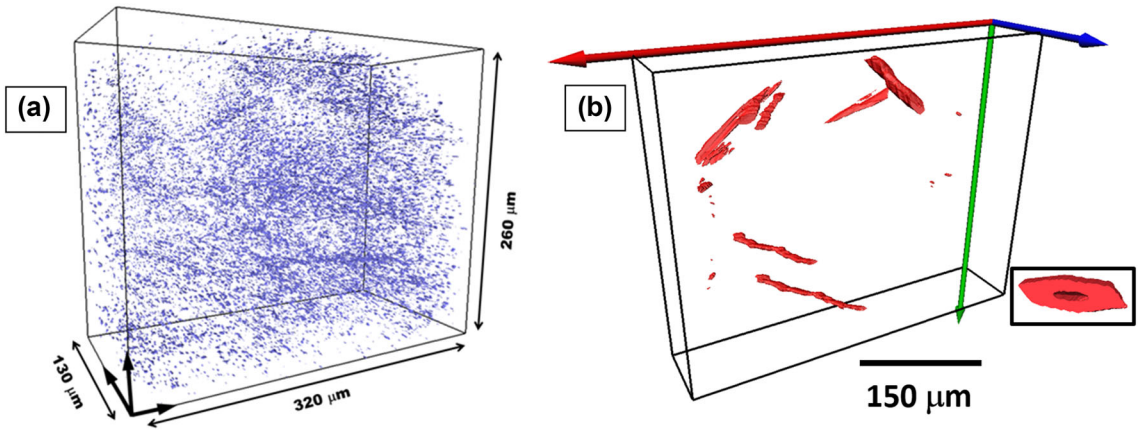

Fig. 6. 3D reconstruction of segmented (a) Cu_6Sn_5 nano-IMCs and (b) Cu_6Sn_5 hexagonal needle IMCs with a magnified cross-section showing the hollow needle morphology.

Table II. 3D quantification results of the Cu_6Sn_5 IMC needles

Volume fraction	**3.1%**
Mean aspect ratio	3.4 ± 1.8
Max length	>150 μm

2, however, is more non-directional but still shows selective segregation of clusters at locations which were found to be triple points in grain boundaries. The volume fraction of these two volumes were fairly close at 2.1% and 1.6% for regions 1 and 2, respectively. The mean aspect ratio was 1.8 ± 0.4, which verifies the nearly spherical morphology observed.

The extensive 3D reconstruction and quantification analysis carried out on the Sn grains and IMC phases can be utilized for several computational modeling studies on predicting the time-dependent evolution of microstructure under external stimuli. As an addendum to this study, statistical information on grain morphology, orientation and spatial distribution of IMC particles were extracted from single 2D EBSD and BSE micrographs, and virtual 3D microstructures were stochastically reconstructed using two-point correlation functions.[19] Considering the highly heterogeneous microstructure, a multi-scale computational procedure was adopted and the accuracy of reconstruction was compared with the experimental volume obtained via serial sectioning.

CONCLUSION

A multi-scale methodology to conduct 3D characterization of Sn grain crystallography and Cu_6Sn_5 intermetallics was presented by coupling EBSD imaging, FIB-SEM imaging, and serial sectioning technique. Reconstruction and visualization of true 3D morphologies of the Sn grains and Cu-$_6Sn_5$ intermetallics within the solder was conducted. A 3D EBSD reconstructed volume measuring 320 μm × 290 μm × 130 μm, was quantified for the grain aspect ratio as a function of position of the Sn grains from either Cu interface, and the influence of local cooling rate differences was elucidated. Grain boundary misorientation distribution showed that 38% of the boundaries were low angle ($<15°$) and that the majority of these were present near the elongated grains at the Cu interface.

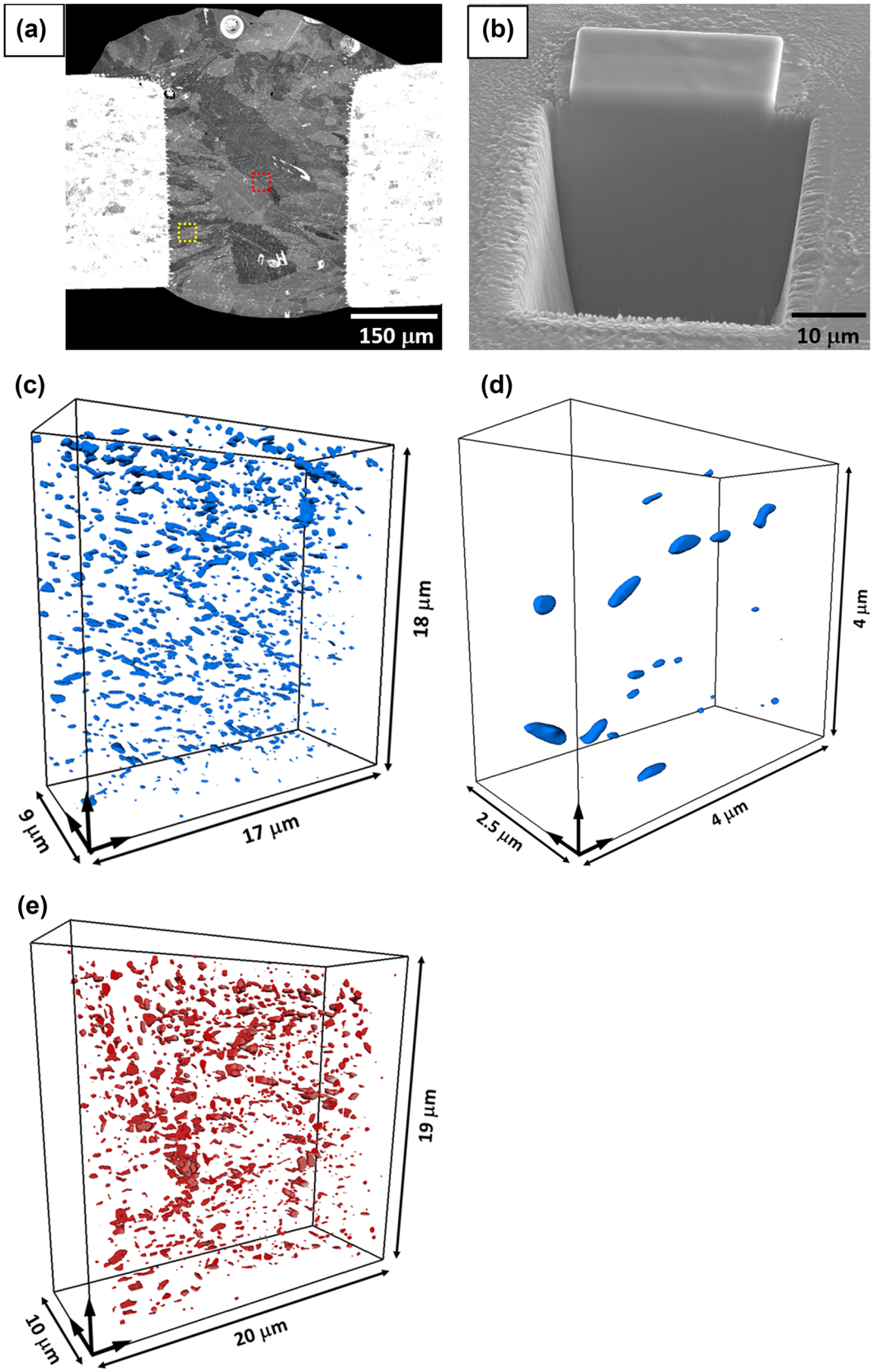

Fig. 7. (a) Ion channeling image of a 250-μm pure Sn solder joint showing Tin grain contrast. Two dotted boxes, one close to the interface and the other at the center, mark the areas from where FIB serial sectioning was carried out. (b) FIB trench is milled in front of the region of interest after thin platinum layer deposition. (c) Cu_6Sn_5 IMC distribution at region 1 (closer to Cu interface). (d) Magnified region within region 1 showing nearly spherical morphology of Cu_6Sn_5 nano-IMCs. (e) Cu_6Sn_5 IMC distribution at region 2 (closer to the center of the solder joint).

3D visualization and quantification of Cu_6Sn_5 nanosized IMCs and hollow hexagonal needles yielded volume fractions of 1.67% and 3.1%, respectively. True morphology of the nano-IMCs was further investigated using FIB-serial sectioning and a mean aspect ratio of 1.8 ± 0.4 verified the nearly spherical morphology of the nanosized particles. While 2D analysis gave us an idea of the heterogeneity of solder microstructures, performing 3D quantification of morphology and distribution proved to be very valuable for better understanding the microstructural evolution in small scale solder joints.

ACKNOWLEDGEMENTS

The authors gratefully acknowledge financial support from the Semiconductor Research Corporation (Dr. John Candelaria, program manager) and the facilities at the LeRoy Eyring Center for Solid State Sciences at Arizona State University. The authors also acknowledge the valuable discussions and suggestions from James Mertens, Sudhanshu Singh, Carl Mayer, Jason Williams, and Shashank Kaira in the Chawla Research group at Arizona State University.

REFERENCES

1. E.P. Wood and K.L. Nimmo, *J. Electron. Mater.* 23, 709 (1994).
2. A.D. Rollett, D.J. Srolovitz, M.P. Anderson, and R.D. Doherty, *Acta Metall. Mater.* 40, 3475 (1992).
3. D. Fan, L.-Q. Chen, and S.-P.P. Chen, *J. Am. Ceram. Soc.* 81, 526 (1998).
4. E.A. Holm and C.C. Battaile, *JOM* 53, 20 (2001).
5. M. Lu, D.-Y. Shih, P. Lauro, C. Goldsmith, and D.W. Henderson, *Appl. Phys. Lett.* 92, 211909 (2008).
6. L.P. Lehman, R.K. Kinyanjui, J. Wang, Y. Xing, L. Zavalij, P. Borgesen, and E.J. Cotts., in *IEEE Electronic Components and Technology Conference.* (2005). doi:10.1109/ECTC.2005.1441341.
7. P. Zimprich, U. Saeed, A. Betzwar-Kotas, B. Weiss, and H. Ipser, *J. Electron. Mater.* 37, 102 (2007).
8. L.M. Yin, X.P. Zhang, and C. Lu, *J. Electron. Mater.* 38, 2179 (2009).
9. J. Cugnoni, J. Botsis, and J. Janczak-Rusch, *Adv. Eng. Mater.* 8, 184 (2006).
10. J.C.E. Mertens, A. Kirubanandham, and N. Chawla, *Microelectron. Reliab.* 55, 2345 (2015).
11. J.C.E. Mertens, A. Kirubanandham, and N. Chawla, *Acta Mater.* 102, 220 (2016).
12. R. Sidhu and N. Chawla, *Mater. Charact.* 52, 225 (2004).
13. M.A. Dudek and N. Chawla, *Acta Mater.* 57, 4588 (2009).
14. H.X. Xie, D. Friedman, K. Mirpuri, and N. Chawla, *J. Electron. Mater.* 43, 33 (2013).
15. D. Frear, D. Grivas, and J.W. Morris, *J. Electron. Mater.* 16, 181 (1987).
16. L.P. Lehman, Y. Xing, T.R. Bieler, and E.J. Cotts, *Acta Mater.* 58, 3546 (2010).
17. L.P. Lehman, S.N. Athavale, T.Z. Fullem, A.C. Giamis, R.K. Kinyanjui, M. Lowenstein, K. Mather, R. Patel, D. Rae, J. Wang, Y. Xing, L. Zavalij, P. Borgesen, and E.J. Cotts, *J. Electron. Mater.* 33, 1429 (2004).
18. P. Borgesen, T.R. Bieler, L.P. Lehman, and E.J. Cotts, *MRS Bull.* 32, 360 (2007).
19. S. Chen, A. Kirubanandham, N. Chawla, and Y. Jiao, *Metall. Mater. Trans. A* 47, 1440 (2015).